JOURNAL OF SPACECRAFT AND ROCKETS
Vol. 44, No. 1, January–February 2007

Simulation and Analyses of Stage Separation of Two-Stage Reusable Launch Vehicles

Bandu N. Pamadi*
NASA Langley Research Center, Hampton, Virginia 23681
Thomas A. Neirynck†
George Washington University, Hampton, Virginia 23666
and
Nathaniel J. Hotchko,‡ William I. Scallion,§ Kelly J. Murphy,§ and Peter F. Covell¶
NASA Langley Research Center, Hampton, Virginia 23681

DOI: 10.2514/1.17896

The development of methodologies, techniques, and tools for analysis and simulation of stage separation is critically needed for successful design and operation of next-generation reusable launch vehicles. As a part of this activity, the ConSep simulation tool is being developed, which is a MATLAB-based front and back end to the commercially available ADAMS solver, an industry standard package for solving multibody dynamic problems. This paper discusses the application of ConSep to the simulation and analysis of staging maneuvers of two-stage-to-orbit bimese reusable launch vehicles, one staging at Mach 3 and the other at Mach 6. The proximity and isolated aerodynamic database were assembled using available wind-tunnel test data. The effects of parametric variations in mass, inertia, flight path angle, and altitude from their nominal values at staging were evaluated. Monte Carlo runs were performed for Mach 3 staging to evaluate the sensitivity to uncertainties in aerodynamic coefficients.

Nomenclature

C_A	=	axial force coefficient
C_m	=	pitching moment coefficient
C_{m_q}	=	damping in pitch derivative, per radian
C_N	=	normal force coefficient
F_x, F_z	=	aerodynamic forces in axial and normal directions, lb
h	=	altitude, ft
I_{xx}, I_{yy}, I_{zz}	=	moment of inertia about the body x, y, and z axes
k_1	=	interpolation constant
k_α, k_q	=	angle of attack and pitch rate feedback gains
L	=	body length, ft
l_{ref}	=	reference length, ft
M	=	aerodynamic pitching moment, lb · ft
M_∞	=	freestream Mach number
q	=	pitch rate, rad/s
q_∞	=	freestream dynamic pressure, lb/ft^2
S_{ref}	=	reference area, ft^2
V_∞	=	freestream velocity, ft/s
x_{cg}	=	x location of center of gravity, ft
z_{cg}	=	z location of center of gravity, ft
α	=	angle of attack, deg
γ	=	flight path angle, deg
$\Delta\alpha$	=	relative difference in angle of attack, deg
Δx, Δz	=	relative axial and normal distances during separation, ft
δ_e	=	elevon deflection, deg
$\delta_{e,\text{bias}}$	=	feedforward elevon deflection, deg
ρ_∞	=	freestream density, slugs/ft^3

Presented as Paper 3247 at the AIAA/CIRA International Space Planes and Hypersonic Systems and Technologies, Capua, Italy, 16–20 May 2005; received 26 May 2005; revision received 24 April 2006; accepted for publication 25 April 2006.

*Aerospace Engineer, Vehicle Analysis Branch. Associate Fellow AIAA.
†Graduate Student, 303 Butler Farm Road, Suite 101 A.
‡Currently Project Engineer, Analytical Mechanics Associates, 17 Research Drive, Hampton, VA 23666-1307. Member AIAA.
§Aerospace Engineer, Aerothermodynamics Branch.
¶Aerospace Engineer, Vehicle Analysis Branch. Senior Member AIAA.

I. Introduction

THE problem of dynamic separation of two bodies within the atmosphere is complex and challenging. One problem that has received significant attention in the literature is that of store separation from the aircraft [1]. The aerodynamic characteristics of the relatively small-sized store are influenced by the proximity of the aircraft, but those of the aircraft are virtually not affected. A similar example is the separation of the X-15 research vehicle from the B-52 carrier aircraft [2]. Here, the aerodynamic characteristics of the relatively smaller X-15 vehicle are influenced by the proximity of the B-52 aircraft, but not vice versa. The other class of stage-separation problem involves separation of two vehicles of comparable sizes for which the aerodynamic characteristics of one vehicle are influenced by the proximity to the other vehicle. However, in some cases, the integrity of only one vehicle may be of importance, such as the staging of multistage expendable launch vehicles. The integrity of only the upper stages is of primary concern postseparation. The expended stages need only to move away safely from the upper stages before their eventual disintegration. For multistage reusable launch vehicles, the integrity of each stage is important postseparation.

NASA studies conducted by Decker et al. [3–7] on stage separation of multistage reusable launch vehicles date back to the early 1960s. These studies addressed the problem of separation of generic two-stage reusable launch vehicles. Wind-tunnel tests were conducted to evaluate the mutual aerodynamic interference between the two stages for supersonic/hypersonic speeds. However, the test data were limited to very few longitudinal and normal separation distances. Also, the simulation did not include the attachment between the stages and the release mechanism. Recent NASA studies by Naftel et al. [8–10] consider Mach 3 staging of two wing-body vehicles. They modeled the attachment of stages, the release mechanism in their simulations, and used active control during separation, but their aerodynamic data did not include the mutual interference effects. They used freestream aerodynamic data for each vehicle.

The interest in stage-separation research returned when it was realized during early 2000 that the technologies needed for the

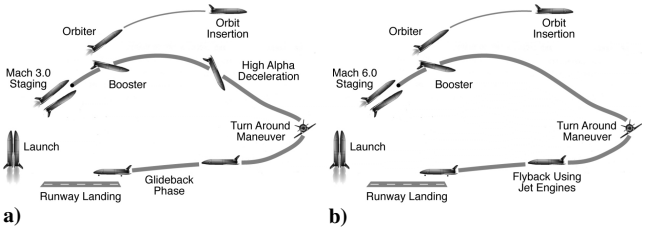

Fig. 1 Schematic illustration of staging flight profiles for a) Mach 3 and b) Mach 6 .

development of next-generation reusable SSTO vehicle are not yet available, and NASA's Next Generation Launch Technology (NGLT) program identified stage separation as one of the critical technologies needed for successful development and operation of next-generation multistage reusable launch vehicles. As a step toward developing this critically needed technology, NASA has initiated comprehensive stage-separation tool development activity that includes wind-tunnel testing as well as development and validation of CFD and engineering-level tools. The stage-separation analysis and conceptual simulation (ConSep) tool is being developed as a part of this activity. The reusable booster, a product of the NASA in-house small launcher vehicle concept study [11], is used in a bimese configuration as the baseline vehicle in this tool development activity. This reusable booster concept is referred to as the Langley glideback booster (LGBB) [11]. Stage-separation wind-tunnel tests were conducted on the LGBB-bimese models at supersonic ($M_\infty = 2.3$, 3.0, and 4.5) and hypersonic ($M_\infty = 6$) Mach numbers to provide data for CFD code development and validation. An overview of NASA's stage-separation tool development activity is presented in [12].

The objective of this paper is to demonstrate the application of ConSep for the stage separation of two-stage-to-orbit (TSTO) reusable launch vehicles. For this purpose, the staging of two LGBB-bimese reusable vehicle concepts are considered: one stages at Mach 3 with booster glideback to launch site and the other stages at Mach 6 with a booster that flies back to the launch site using air-breathing jet engines. The two flight profiles are illustrated in Fig. 1. The simulation and analyses performed in this study are limited to these two stage-separation events. Any abort separations that may occur at other conditions are not addressed. The ascent and glideback/flyback trajectories are not addressed here. The initial conditions for the staging maneuvers are based on the available ascent trajectories of similar vehicles staging at Mach 3 and Mach 6. For each vehicle, the aerodynamic database was assembled from the wind-tunnel test data generated as part of the stage-separation tool development activity. These two databases include the static longitudinal aerodynamic coefficients for proximity conditions and interference-free or isolated conditions. In this study, only longitudinal motion during stage separation is discussed. The lateral/directional motion is not addressed in this study.

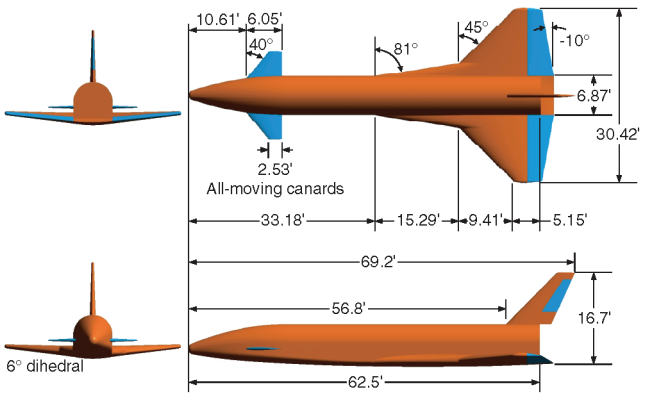

Fig. 2 Three-view diagram of the Langley glideback booster (LGBB).

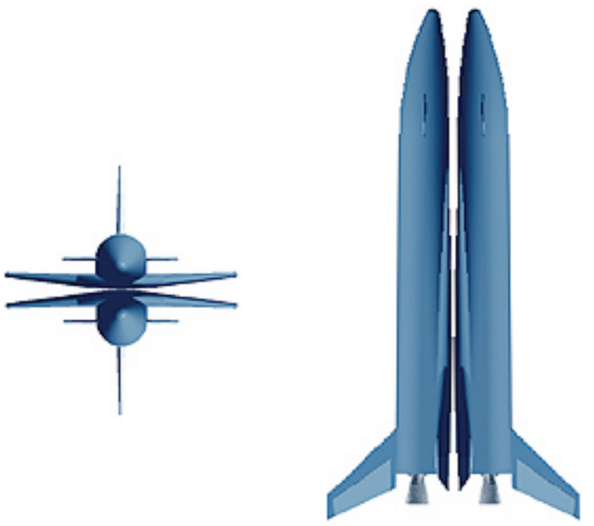

Fig. 3 Schematic diagram of the LGBB-bimese vehicle.

It was found that aerodynamic separation is feasible for a Mach 3 staging LGBB-bimese vehicle. The booster and orbiter could be safely separated using a simple active (closed-loop feedback) control of aerodynamic surfaces (elevons). However, for a Mach 6 LGBB-bimese vehicle, aerodynamic separation was not feasible and separation motors were used to accomplish safe separation. This study also discusses the effect of variations in mass, inertia, altitude, and flight path angle at staging on the vehicle motion during stage separation. To evaluate the sensitivity of the vehicle motion to uncertainties in aerodynamic coefficients, Monte Carlo studies were performed for the LGBB-bimese Mach 3 stage separation. Some early results of this study were presented in [13].

II. Vehicle Description

The TSTO vehicles used in this study are bimese concepts, in which both the booster and the orbiter have the same outer mold lines. However, the "true" bimese vehicles are identical internally and externally, to the extent that the role of the booster and orbiter can be switched. For the bimese vehicles used in this study, the outer mold lines of both the booster and orbiter are identical to that of the LGBB of the small launcher [11] shown in Fig. 2. However, the LGBB-bimese vehicles do not feature canards. Furthermore, both the LGBB-bimese booster and orbiter are approximately 4.16 times larger in size than the LGBB of the small launcher. A schematic arrangement of the belly-to-belly LGBB-bimese configuration is presented in Fig. 3.

The sizing of the two LGBB-bimese vehicles used in this study was based on Mach 3 glideback and Mach 5 flyback reference configurations developed during the NASA Intercenter Systems Analysis Team (ISAT) effort, which was part of the Space Launch Initiative (SLI) program [14]. The LGBB-bimese vehicles are sized for a 35,000-lb payload to the International Space Station (ISS). For

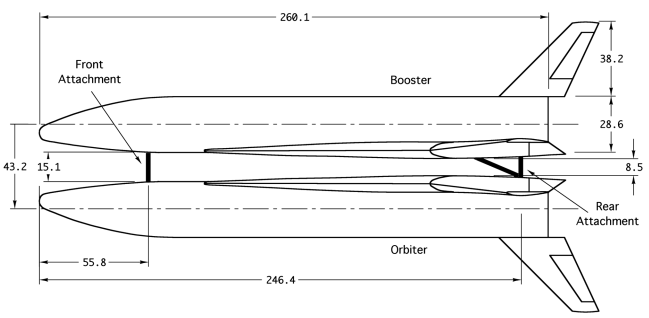

Fig. 4 Schematic illustration of the attachment of the booster and the orbiter (all dimensions in feet).

Table 1 Mass properties at staging for the Mach 3 LGBB-bimese vehicle

Property	Orbiter	Booster
Weight, lb	2.909×10^6	300,000
Total thrust, lb	4.879×10^6	0
x_{cg}, ft	197.6	130.0
I_{xx}, slugs · ft^2	20.9×10^6	3.36×10^6
I_{yy}, slugs · ft^2	245×10^6	39.4×10^6
I_{zz}, slugs · ft^2	245×10^6	39.4×10^6

Table 2 Mass properties at staging for the Mach 6 LGBB-bimese vehicle

Property	Orbiter	Booster
Weight, lb	2.23×10^6	476,000
Total thrust, lb	4.899×10^6	0
x_{cg}, ft	197.6	130.0
I_{xx}, slugs · ft^2	16×10^6	5.33×10^6
I_{yy}, slugs · ft^2	188×10^6	62.6×10^6
I_{zz}, slugs · ft^2	188×10^6	62.6×10^6

the purpose of this study, the space shuttle main engine (SSME) class engines were used for each stage.

The schematic diagram of the attachment of the orbiter to the booster is shown in Fig. 4. The booster is attached to the orbiter at two points. Before the release, the forward joint is assumed to be a fixed support and the aft joint is assumed to permit rotation in pitch. These struts and the gap measurements are similar in geometry to the shuttle orbiter and external tank attachment system, except that the rear strut has a pivot linkage that allows the rotation of the booster relative to the orbiter upon release of the forward joint. This separation sequence is similar to that used in [10]. At separation, the orbiter is operating at full thrust and the booster at no thrust. The estimated mass properties of the two vehicles at staging are presented in Tables 1 and 2.

A. Proximity Aerodynamic Characteristics and Development of Aerodynamic Database

The longitudinal stage-separation aerodynamic coefficients depend on the relative location of the two vehicles as characterized by three variables Δx, Δz, and $\Delta\alpha$. The dependence of stage-separation aerodynamic coefficients on Δx, Δz, and $\Delta\alpha$ is in addition to their usual dependence on Mach and α. Sketches showing the relative locations of the two vehicles in the wind-tunnel tests and corresponding orientations in flight are presented in Fig. 5. The separation distances Δx and Δz are measured with respect to the orbiter coordinate system. Note that Δx is negative when the booster is aft of the orbiter.

The proximity aerodynamic database was developed using the data from the stage-separation wind-tunnel tests conducted in the NASA Langley unitary plan wind tunnel (UPWT) at Mach 3 and in their 20-in. Mach 6 tunnel. Some Mach 3 stage-separation tests were also conducted in the Aerodynamic Research Facility (ARF) at the NASA Marshall Space Flight Center (MSFC). The MSFC test data [14] were used as a reference but not in the development of the aerodynamic database discussed in this study. A brief description of the Langley stage-separation tests in the UPWT and the 20-in. Mach 6 tunnel is presented in this paper. Detailed descriptions of the test facilities, support hardware, models, instrumentation, and test procedure are available in [12]. All stage-separation wind-tunnel tests were conducted for power-off conditions. The test data were not adjusted for orbiter power-on conditions at staging, and any errors due to this discrepancy were not addressed in this study. The incremental aerodynamic coefficients for the elevon deflections in proximity conditions were not available for either of the stage-separation tests. In view of this, Mach 3 elevon deflection data obtained from isolated LGBB model tests in the Langley UPWT (Mach range: 1.6 to 4.5) was used. Such isolated LGBB elevon data for Mach 6 were not available. In the absence of a better alternative, the available Mach 4.5 UPWT elevon deflection data were used as applicable for Mach 6 conditions. It is possible that isolated elevon incremental coefficients differ from those in proximity. This issue was not addressed in this study.

The Mach 3 stage-separation tests were conducted in NASA Langley UPWT facility. The UPWT is a closed-circuit, continuous flow, pressure tunnel with two test sections that are nominally 4 ft^2 in cross section and 7-ft long. The Mach number range is 1.5 to 2.86 in test section 1 and 2.3 to 4.63 in test section 2. Two LGBB 1.75% scale models were used. These correspond to 0.426% scale models of the LGBB-bimese vehicles. One LGBB model designated as the orbiter (bottom) model was always held at a fixed location and held fixed at $\alpha = 0$. The other test model designated as the booster (top) model was moved in the x (aft) and in z (vertical) directions. All the x and z traverses were done for two values of angle of attack, 0 and 5 deg. A schematic illustration of the LGBB-bimese Mach 3 test matrix is presented in Fig. 6.

The Mach 6 stage-separation tests were conducted in the Langley 20-in. Mach 6 tunnel. Two 1.21% scale LGBB models (0.2909% LGBB-bimese) were used, one as a booster model and the other as an orbiter model. All x movements were achieved by moving the booster (top) model aft of the orbiter (bottom) model, and z movements were achieved by lowering the orbiter model from the mated position. All x and z separations were run at $\Delta\alpha = 0$ and 5 deg. At each of the nominal x and z locations, both models were

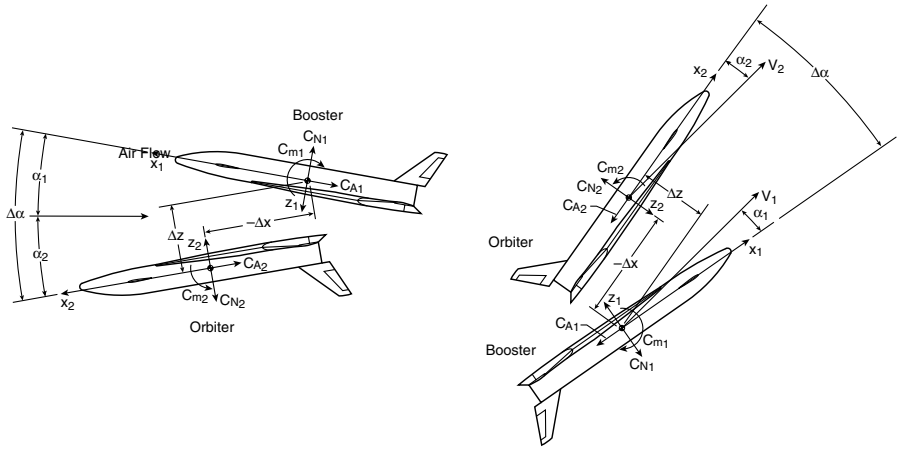

a) Wind tunnel tests **b) Flight**

Fig. 5 Relative locations of the booster and orbiter in proximity.

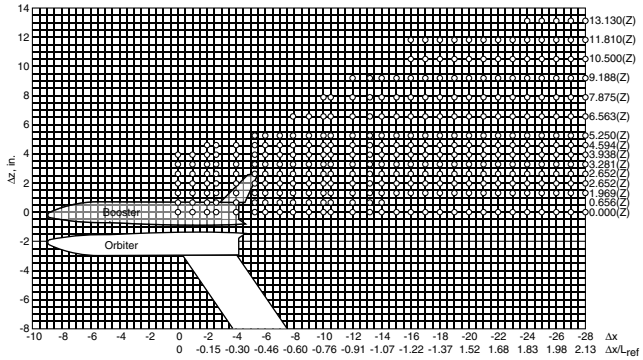

Fig. 6 Schematic illustration of LGBB-bimese UPWT test matrix at Mach 3.

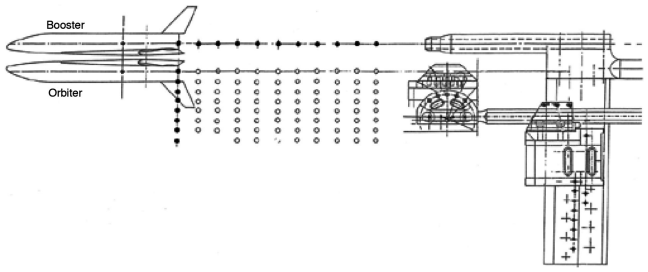

Fig. 7 Schematic illustration of the LGBB-bimese Mach 6 tunnel test matrix.

simultaneously swept through an angle of attack range using the tunnel strut angle of attack mechanism so that α varied for each model, whereas $\Delta\alpha$, Δx, and Δz remain fixed at their nominal values. However, for $\Delta\alpha = 5$ deg, the actual values Δx and Δz are slightly different due to the rotation in pitch. The angle of attack range was about -7 to $+7$ deg. A schematic illustration of the LGBB-bimese Mach 6 test matrix is presented in Fig. 7.

It is necessary to note that for stage-separation wind-tunnel testing, the direction and magnitude of velocity are identical for both orbiter and booster models. In actual flight postseparation, this is not always true. The differences in velocity magnitudes amount to differences in flight Mach numbers and the differences in directions amount to differences in flight path angles. Therefore, some errors are likely to be introduced in the simulations based on these stage-separation wind-tunnel test data, especially if the Mach numbers and flight path angles of the two separating vehicles differ considerably.

Table 3 Summary of wind-tunnel test parameters

Parameter	UPWT	20-in. Mach 6 tunnel
Mach number	3.0	6.0
Reynolds number, 10^6/ft	1.0 to 4.0	0.5 to 0.9
Moment reference point	0.68 L	0.68 L
α (orbiter), deg	0.0	-7.0 to $+7.0$
α (booster), deg	0, 5.0	-7.0 to $+7.0$
$\Delta\alpha$, deg	0, 5.0	0, 5.0
$\Delta x/l_{\text{ref}}$	0 to -2.1	0 to -1.0
$\Delta z/l_{\text{ref}}$	0 to 1.0	0 to 0.5

The test parameters for Mach 3 and Mach 6 stage-separation tests are summarized in Table 3. The separation distances Δx are negative in Table 3 because the booster was always located aft of the orbiter.

To illustrate the physical nature of aerodynamic interference, sample schlieren photographs are presented in Figs. 8 and 9. In the mated condition $\Delta x = \Delta z = 0$ for $\Delta\alpha = 0$, the mutual interference is characterized by a channel-like flow between the two bodies and the bow shock waves of each body impinge on the other, resulting in multiple reflections. As the two bodies move a short distance apart in the x and z directions, the channel-like flow is not observed. Instead, the mutual interference is mainly determined by bow shock impingements and their reflections. The data show that the orbiter falls out of the booster's influence much earlier than the booster goes out of the orbiter's influence. For example, for $\Delta x = -0.4$ and $\Delta z = 0.25$, the orbiter is nearly out of the booster's influence, whereas the booster is still under the orbiter's influence. The shock intersections affect surface pressure distribution, causing it to rise over the downstream part of the body, resulting in significant variations in normal force and pitching moment coefficients. The flow pattern over the LGBB-bimese models at Mach 6 has similar features, but shock angles are much steeper, as shown in Fig. 9.

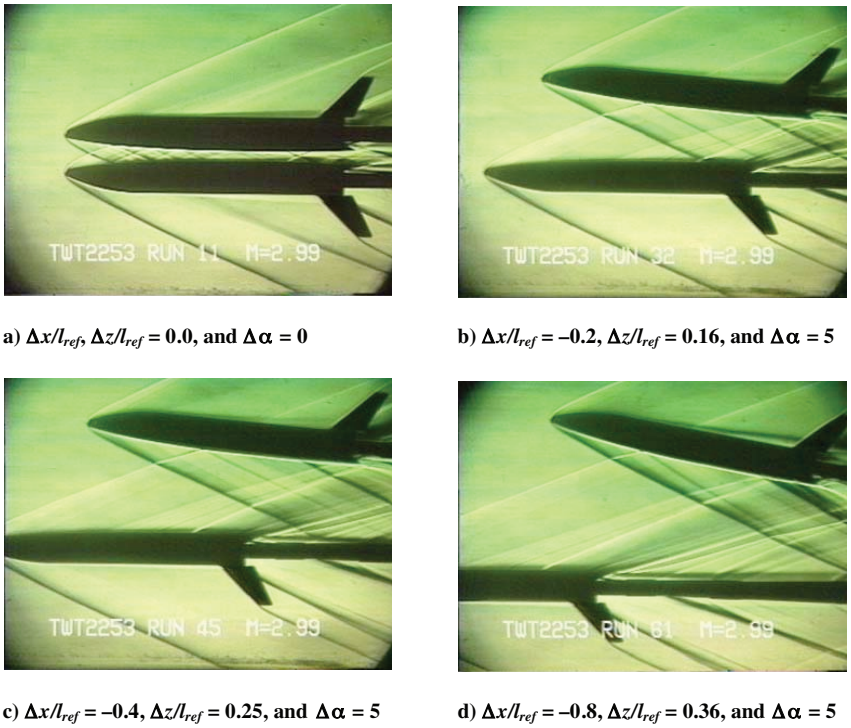

a) $\Delta x/l_{ref}$, $\Delta z/l_{ref}$ = 0.0, and $\Delta\alpha$ = 0

b) $\Delta x/l_{ref}$ = –0.2, $\Delta z/l_{ref}$ = 0.16, and $\Delta\alpha$ = 5

c) $\Delta x/l_{ref}$ = –0.4, $\Delta z/l_{ref}$ = 0.25, and $\Delta\alpha$ = 5

d) $\Delta x/l_{ref}$ = –0.8, $\Delta z/l_{ref}$ = 0.36, and $\Delta\alpha$ = 5

Fig. 8 Mach 3 schlieren photographs of the LGBB-bimese configuration in the MSFC Aerodynamic Research Facility [4].

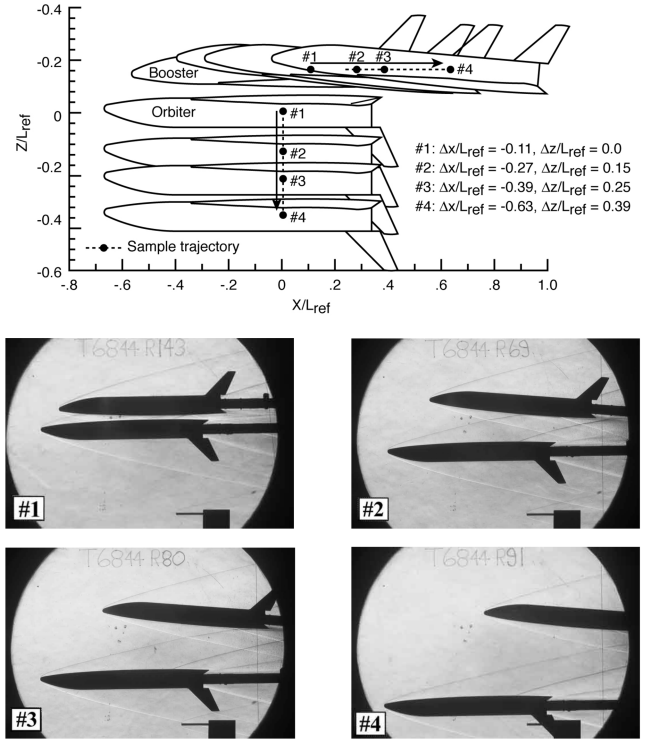

Fig. 9 Schlieren photographs of the LGBB-bimese configuration in the 20-in.Mach 6 tunnel.

The isolated LGBB aerodynamic coefficients at Mach 3 and Mach 6 are presented in Fig. 10. To illustrate the physical nature of variation of longitudinal aerodynamic coefficients in proximity, the wind-tunnel test data for $\alpha = 0$ and $\Delta\alpha = 0$ are presented in this paper. In Figs. 11–16, the total coefficients are presented for the Mach 3 case. However, the test data for Mach 6 were in the form of incremental coefficients with respect to the corresponding isolated

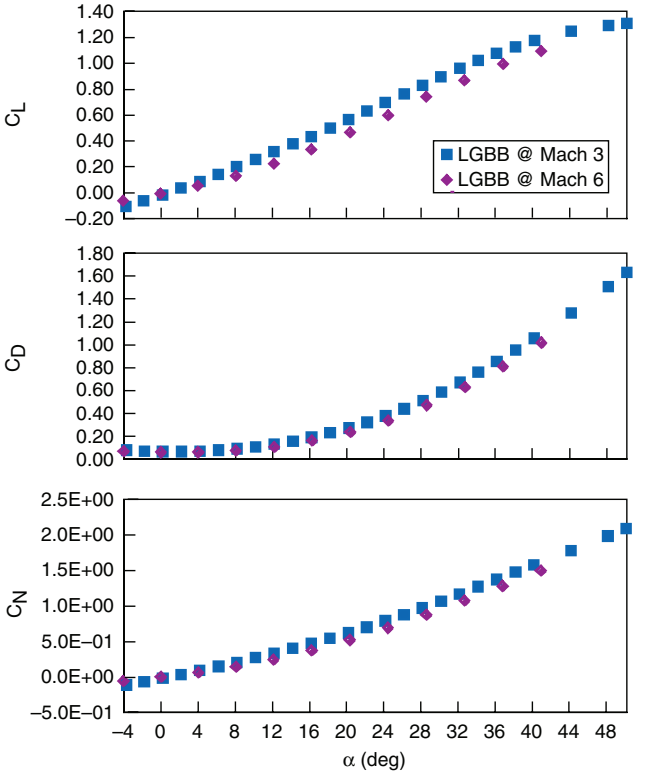

Fig. 10 Isolated LGBB lift, drag, and pitching moment coefficients at Mach 3 and Mach 6.

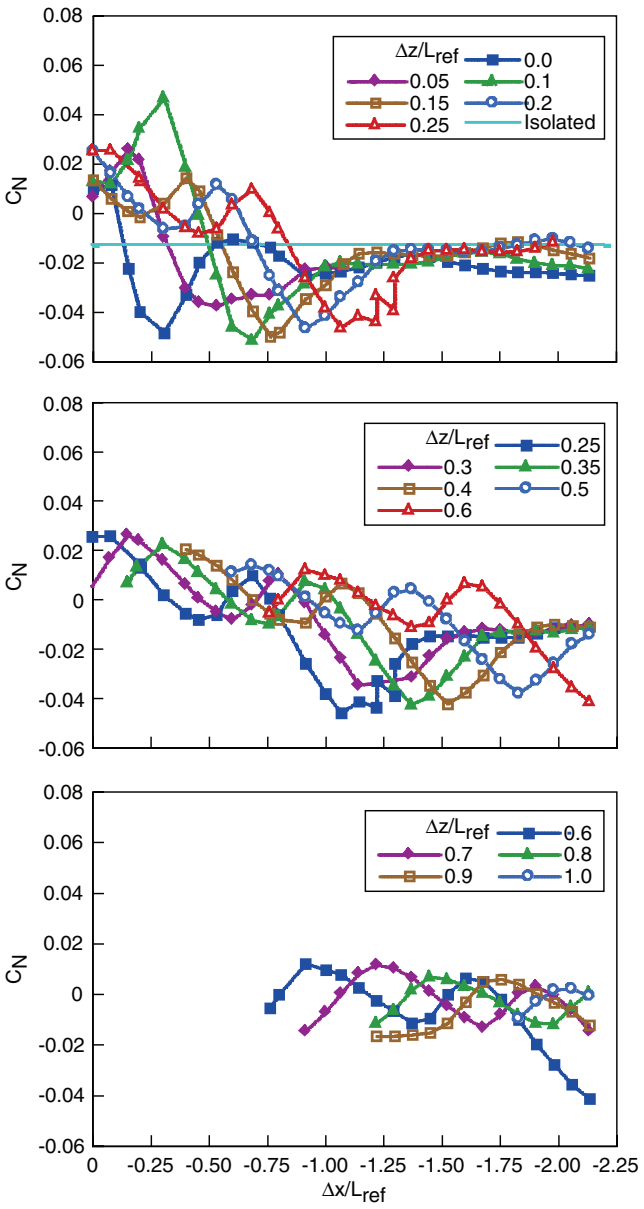

Fig. 11 Variation of the booster normal force coefficient with $\Delta x/L_{\text{ref}}$ and $\Delta z/L_{\text{ref}}$ at Mach 3 for $\alpha = 0$ and $\Delta\alpha = 0$ deg.

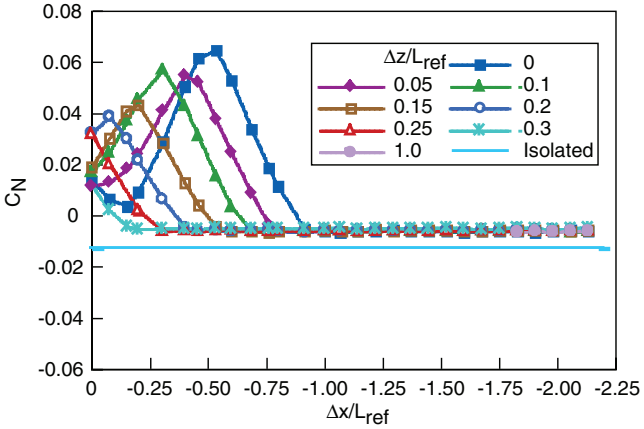

Fig. 12 Variation of the orbiter normal force coefficient with $\Delta x/L_{\text{ref}}$ and $\Delta z/L_{\text{ref}}$ at Mach 3 for $\alpha = 0$ and $\Delta\alpha = 0$ deg.

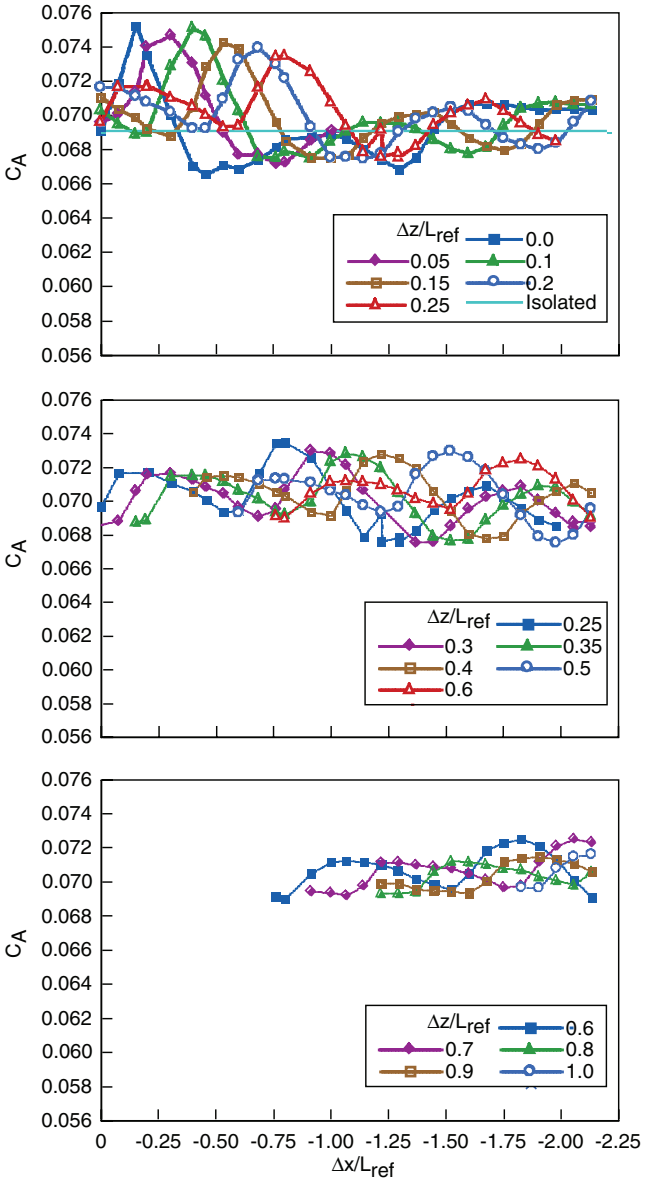

Fig. 13 Variation of the booster axial force coefficient with $\Delta x/L_{\text{ref}}$ and $\Delta z/L_{\text{ref}}$ at Mach 3 for $\alpha = 0$ and $\Delta\alpha = 0$ deg.

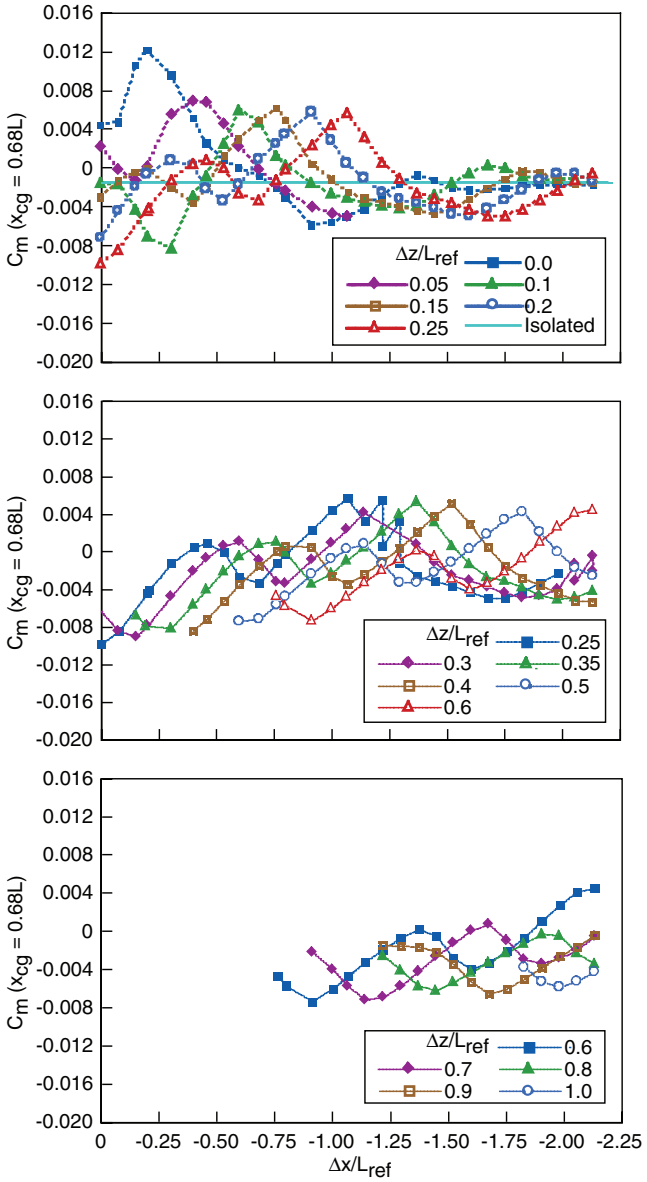

Fig. 14 Variation of the booster pitching moment coefficient with $\Delta x/L_{\text{ref}}$ and $\Delta z/L_{\text{ref}}$ at Mach 3 for $\alpha = 0$ and $\Delta\alpha = 0$ deg.

condition, and these incremental coefficients are presented in Fig. 17. The Mach 3 proximity aerodynamic coefficients of the orbiter (Figs. 12, 15, and 16) do not approach the corresponding isolated values, because the support structures used in proximity wind-tunnel tests and isolated wind-tunnel tests were slightly different. The test data were not corrected for these differences. Any errors due to this discrepancy were not addressed in this study.

B. Simulation of Staging Maneuvers

The simulation of staging maneuvers was done using the automatic dynamic analysis of mechanical systems (ADAMS) solver, an industry-standard package for solving multibody dynamic problems [15]. The user does not have to input the governing equations of motion to ADAMS for vehicle motion during stage separation but needs to provide mathematical models of the aerodynamic and other external forces/moments acting on each of the vehicles during stage separation. ADAMS assembles coupled/constrained equations of motion for each vehicle based on the user-supplied inputs and generates solutions to those equations as users request. To simplify the process of using ADAMS for solving stage-separation problems, NASA Langley has developed a MATLAB-based front and back end, called ConSep to ADAMS solver. ConSep derives its heritage from SepSim, a front and back end to ADAMS for X-43A (hyper-X) stage separation [16]. An independent verification of the SepSim/ADAMS predictions of the X-43A stage separation

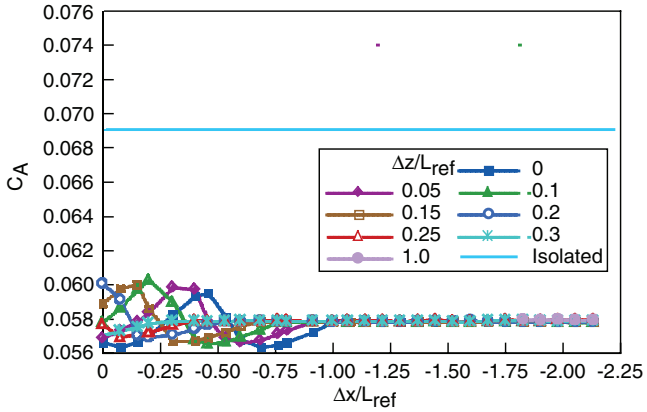

Fig. 15 Variation of the orbiter axial force coefficients with $\Delta x/L_{\text{ref}}$ and $\Delta z/L_{\text{ref}}$ at Mach 3 for $\alpha = 0$ and $\Delta\alpha = 0$ deg.

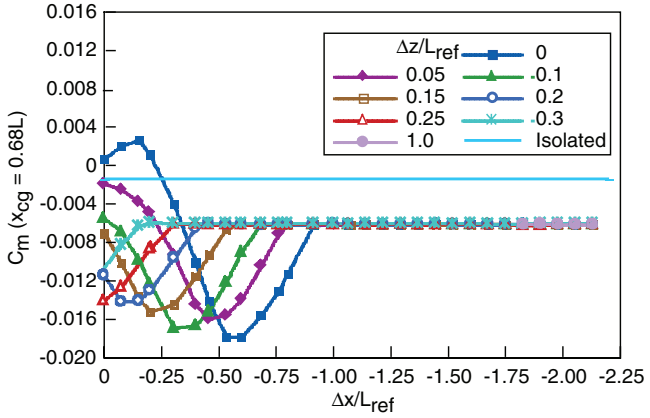

Fig. 16 Variation of the orbiter pitching moment coefficients with $\Delta x/L_{\text{ref}}$ and $\Delta z/L_{\text{ref}}$ at Mach 3 for $\alpha = 0$ and $\Delta\alpha = 0$ deg.

[16] was conducted and the two results were found to be in close agreement. This exercise confirmed that SepSim/ADAMS sets up and solves the equations of motion for stage-separation problems in an acceptable manner. However, such an independent verification of ConSep/ADAMS has, so far, not been performed.

ConSep allows the user to set up the stage-separation problems in a simple manner. It converts the user inputs into the model specifications used by ADAMS, initiates the ADAMS solver, and postprocesses the ADAMS output to express the simulation results in a convenient form. ConSep is designed to allow the user to link aerodynamic mathematical models, aerodynamic data tables, interpolation routines, model attachment points/joints, separation forces due to reaction jets or piston type devices, closed-loop proportional and derivative (PD) control, actuator dynamics, atmospheric winds, engine gimbals, etc., to the ADAMS solver. ConSep is also designed to permit the user to study the effect of variations in selected input parameters and to perform Monte Carlo studies. The main advantage of ConSep is that the user does not have to be trained in ADAMS to use it for solving stage-separation problems. Additional information on ConSep is available in [17].

In this study, simple aerodynamic separation aided by active closed-loop control of elevons on both vehicles was attempted for Mach 3 staging. Separation forces or thrusters were not used. For Mach 6 staging, aerodynamic separation was not feasible and separation thrusters were used. As said earlier, at staging, the orbiter was assumed to be operating at full thrust, but the booster was not. The engine gimbal was not used for control. The staging event starts with the release of the forward joint, permitting the booster to rotate about the aft joint. The aft joint was released when a specified event (such as $\Delta\alpha$ or time reaching a specified value) occurred, allowing the booster to separate. The structural problems that may arise at separation were not addressed in this study.

The inputs to ConSep/ADAMS simulation of LGBB-bimese stage separation were as follows: definition of a body-fixed coordinate system for each vehicle in relation to the ground-fixed system (north-east-down) defined in ADAMS via Euler angles; mass; inertia; center of gravity of each vehicle in its body-fixed coordinate system; initial altitude; velocity; flight path angle; angle of attack of each vehicle; mathematical model of aerodynamic forces and moments in proximity and free flight; location of the moment reference point for each vehicle; tables of proximity aerodynamic forces and moment coefficients as functions of Δx, Δz, α, and $\Delta\alpha$ (for Mach 3 and 6); aerodynamic coefficients for isolated or free-flight conditions at Mach 3 and 6; incremental aerodynamic coefficients for elevon deflections at Mach 3 and 6; atmospheric model; location of the separation motors; magnitude and direction of net thrust; location of joints/attachment points and degrees of freedom for each joint; time/event for the partial/complete release of front and aft joints; models of actuators for aerodynamic control surface (elevons) of each vehicle; gains for the closed-loop PD controller; time for starting and stopping the integration of equations of motion; step size; and accuracy of integration. The initial conditions and other parameters used for the stage-separation simulations are presented in Table 4.

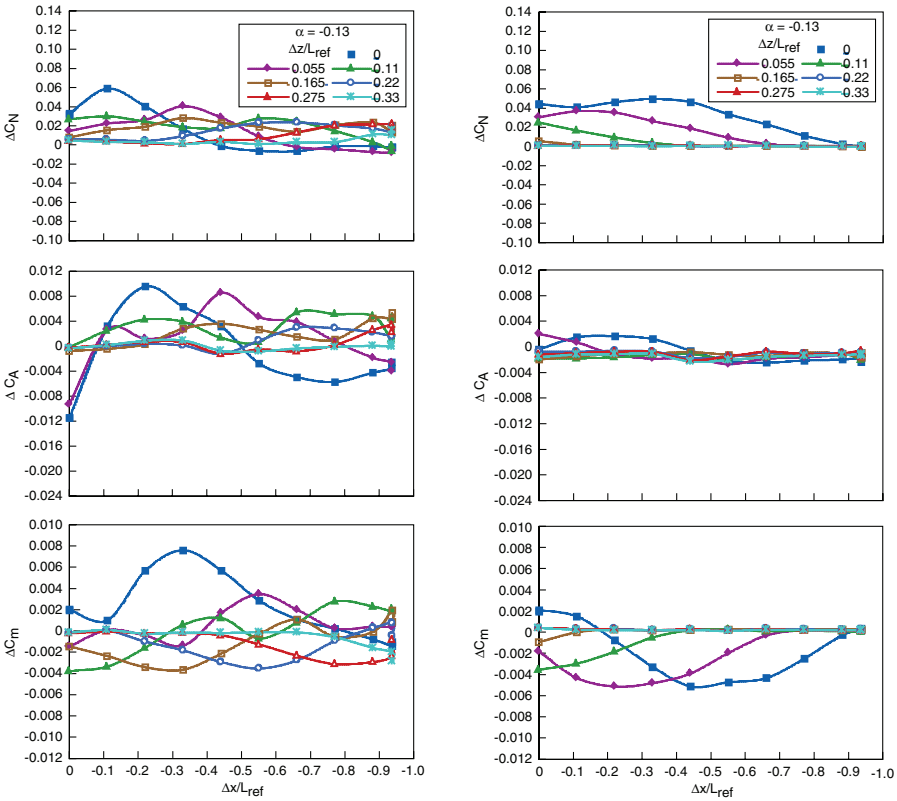

Booster at $\Delta\alpha = 0$ deg **Orbiter at $\Delta\alpha = 0$ deg**

Fig. 17 Proximity aerodynamic coefficients for Mach 6 at $\alpha = 0$ and $\Delta\alpha = 0$ deg.

Table 4 Initial conditions for LGBB-bimese vehicles

Parameter	Mach 3 staging	Mach 6 staging
Altitude, ft	85,000	150,000.0
Velocity, ft/s	2924.6	6586.6
Dynamic pressure, lb/ft^2	287.0	75.0
Flight path angle γ, deg	53.0	30.0
α (booster), deg	0.0	0.0
α (orbiter), deg	0.0	0.0
Atmospheric model	U.S. standard atmosphere 1962	U.S. standard atmosphere 1962
Separation thrust	0.0	750,000.0
Simulation time, s	6.0	6.0
Integration step size, s	0.01	0.01
Front joint release, s	0.1	0.1
Aft-joint rotation, s	0.1	0.1
Aft-joint release, event/time	$\Delta\alpha = 1.0$ deg	$\Delta\alpha = 1.0$ deg (baseline) $t = 0.1$ s (nominal and all other cases)

1. Aerodynamic Forces and Moments

The axial force, normal force and pitching moment are defined as follows:

$$F_x = -\tfrac{1}{2}\rho V^2 S_{\text{ref}} C_A \tag{1}$$

$$F_z = -\tfrac{1}{2}\rho V^2 S_{\text{ref}} C_N \tag{2}$$

$$M = \tfrac{1}{2}\rho V^2 S_{\text{ref}} l_{\text{ref}} C_m \tag{3}$$

where $S_{\text{ref}} = 7527.94$ ft^2 and $l_{\text{ref}} = 260.1$ ft. Note that the body length is used as the reference length. The moment reference point was located at 0.68 l_{ref} from the nose of each vehicle. The Mach number is assumed to be constant during stage separation. With this assumption, the aerodynamic coefficients in proximity during stage separation are functions of the angle of attack; relative angle of attack and separation distances can be expressed as follows:

$$C_{A1p} = C_{A1p}(\boldsymbol{\alpha}_1, \Delta\boldsymbol{\alpha}, \Delta x, \Delta z) + \Delta C_{A1,\delta_{e1}} \tag{4}$$

$$C_{A2p} = C_{A2p}(\boldsymbol{\alpha}_2, \Delta\boldsymbol{\alpha}, \Delta x, \Delta x) + \Delta C_{A2,\delta_{e2}} \tag{5}$$

$$C_{N1p} = C_{N1p}(\boldsymbol{\alpha}_1, \Delta\boldsymbol{\alpha}, \Delta x, \Delta z) + \Delta C_{N1,\delta_{e1}} \tag{6}$$

$$C_{N2p} = C_{N2p}(\boldsymbol{\alpha}_2, \Delta\boldsymbol{\alpha}, \Delta x, \Delta z) + \Delta C_{N2,\delta_{e2}} \tag{7}$$

$$C_{m1p} = C_{m1p}(\boldsymbol{\alpha}_1, \Delta\boldsymbol{\alpha}, \Delta x, \Delta z) + \Delta C_{m1,\delta_{e1}} \tag{8}$$

$$C_{m2p} = C_{m2p}(\boldsymbol{\alpha}_2, \Delta\boldsymbol{\alpha}, \Delta x, \Delta z) + \Delta C_{m2,\delta_{e2}} \tag{9}$$

Here, the suffixes 1 and 2 correspond to the booster and orbiter, respectively. In this paper, the booster is sometimes referred to as vehicle 1 and the orbiter as vehicle 2. The suffix p denotes proximity conditions. When the two vehicles move out of the proximity range and are essentially in isolated or free-flight (no interference) conditions, the aerodynamic coefficients are assumed to be given by

$$C_{A1f} = C_{A1}(\boldsymbol{\alpha}_1) + \Delta C_{A1,\delta_{e1}} \tag{10}$$

$$C_{A2f} = C_{A2}(\boldsymbol{\alpha}_2) + \Delta C_{A2,\delta_{e2}} \tag{11}$$

$$C_{N1f} = C_{N1}(\boldsymbol{\alpha}_1) + \Delta C_{N1,\delta_{e1}} \tag{12}$$

$$C_{N2f} = C_{N2}(\boldsymbol{\alpha}_2) + \Delta C_{N2,\delta_{e2}} \tag{13}$$

$$C_{m1f} = C_{m1}(\boldsymbol{\alpha}_1) + \Delta C_{m1,\delta_{e1}} \tag{14}$$

$$C_{m2f} = C_{m2}(\boldsymbol{\alpha}_2) + \Delta C_{m2,\delta_{e2}} \tag{15}$$

Here, the suffix f denotes isolated or free-flight condition. Note that $C_A = C_{Ap}$ in proximity and $C_A = C_{Af}$ for isolated or free-flight conditions, and so on.

Owing to facility/resource limitations, the Langley Mach 3 and Mach 6 proximity test data do not cover sufficiently large values of Δx and Δz so that the aerodynamic coefficients transition smoothly from stage-separation (proximity) coefficients to isolated (no interference or free-flight) coefficients. In view of this, the following assumption was introduced to transition from the available stage-separation aerodynamic coefficients to the isolated aerodynamic coefficients as the vehicles move apart.

$$C_{A1t} = k_1 C_{A1f} + (1 - k_1) C_{A1p} \tag{16}$$

$$C_{A2t} = k_1 C_{A2f} + (1 - k_1) C_{A2p} \tag{17}$$

$$C_{N1t} = k_1 C_{N1f} + (1 - k_1) C_{N1p} \tag{18}$$

$$C_{N2t} = k_1 C_{N2f} + (1 - k_1) C_{N2p} \tag{19}$$

$$C_{m1t} = k_1 C_{m1f} + (1 - k_1) C_{m1p} \tag{20}$$

$$C_{m2t} = k_1 C_{m2f} + (1 - k_1) C_{m2p} \tag{21}$$

Here, the suffix t denotes the transition region. In the proximity region, $k_1 = 0$, and for isolated or free-flight condition, $k_1 = 1$. In the transition region, k_1 varies linearly from 0 to 1. The transition region is assumed to consist of two concentric ellipses, an inner ellipse and an outer ellipse defined empirically, using the stage-separation test data as guides. Both ellipses are centered at the moment reference point of each vehicle and move with the vehicles. The parameter k_1 is assumed to vary linearly from zero at the inner ellipse to one at the

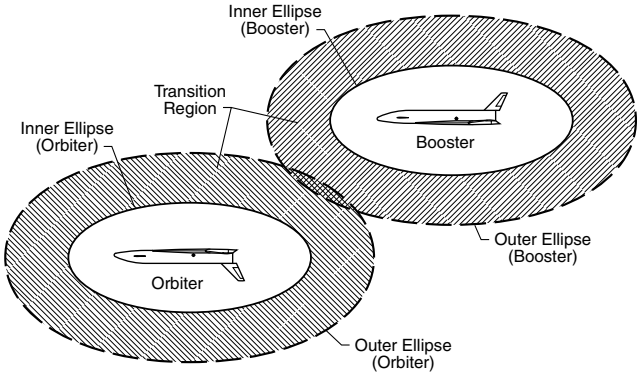

Fig. 18 Concept of transition regions.

outer ellipse. These concepts are illustrated in Fig. 18. Note that the forward halves of the ellipses attached to the orbiter and aft halves attached to the booster are not used in the present implementation of this concept.

2. *Constraints*

The available stage-separation test data are limited in α and $\Delta\alpha$ values, as shown in Table 3. The extrapolation outside the database limits was not permitted. In view of this, a constraint was imposed on simulations that each vehicle's α and $\Delta\alpha$ remain within the limits of the proximity databases, that is, $0 < \alpha \leq 5.0$ deg and $0 < \Delta\alpha \leq 5.0$ deg. However, it is quite possible that safe separations may occur at angles of attack outside the limits of the current proximity database. Because the separation of Mach 3 and Mach 6 bimese vehicles discussed in this paper were test problems to demonstrate the application of ConSep for TSTO staging, the possibility of safe separations outside the database limits were not investigated.

3. *Criteria for Safe Separation*

The criteria for a successful stage separation were as follows: 1) no vehicle recontact and 2) booster stays out of the orbiter's engine plume. It was estimated that the orbiter's plume is correctly expanded for ambient pressure/altitude conditions for both Mach 3 and Mach 6 staging vehicles. Hence, the combined diameter of the orbiter engines would be approximately equal to the vehicle base diameter, which is 28.6 ft. However, to be on the conservative side, the minimum Δz separation to avoid booster contact with orbiter plume is assumed to be equal to two diameters (59.2 ft) or $\Delta z/l_{\text{ref}} \geq 0.219$. For the x separation, the acceptable separation distance was specified as $\Delta x/l_{\text{ref}} \geq 3.0$.

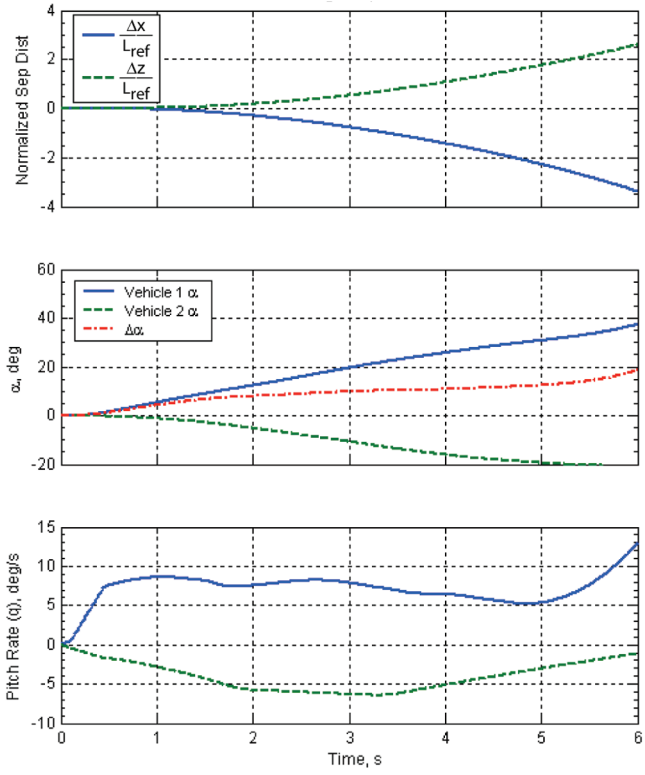

Fig. 19 Mach 3 baseline separation.

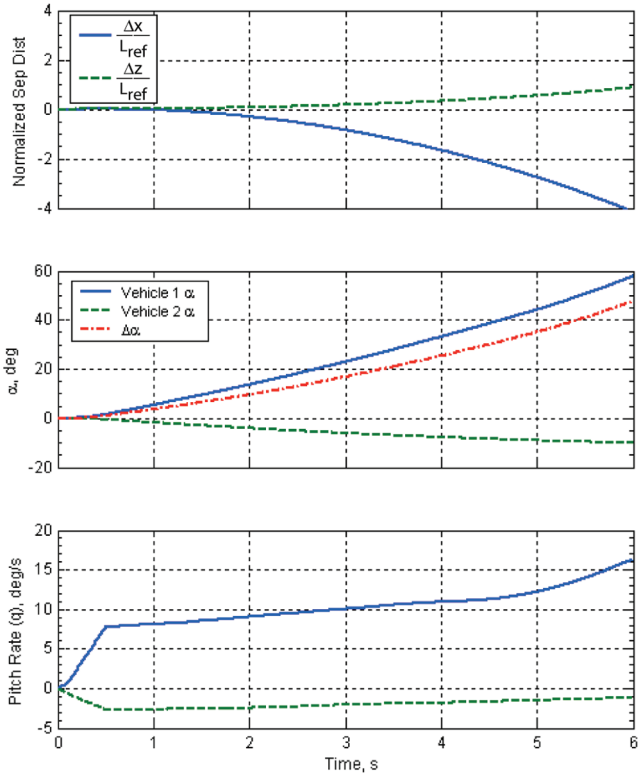

Fig. 20 Mach 6 baseline separation.

It is possible that the impingement of the orbiter engine plume on the separating booster can be tolerated if the resulting aerodynamic heating effects are not critical. In such cases, it is necessary to account for the incremental aerodynamic forces on the booster that are due to orbiter plume impingement during stage separation. However, this issue was not addressed in this study.

4. *Animation of the Stage-Separation Event*

The synergistic engineering environment (SEE) was used to create animations of the staging maneuvers. The SEE used the geometry models of the LGBB and the ConSep output to generate these animations. The geometrical shape of the orbiter engine plume was assumed to be a cylinder of constant diameter equal to base diameter, because the exit plume was assumed to be expanded correctly for both Mach 3 and Mach 6 staging conditions. This plume shape was included in the geometry model of the orbiter. The animation of the staging event provides an effective means for visualization of engine plume interactions or collisions, if any. Additional information on SEE is available in [18].

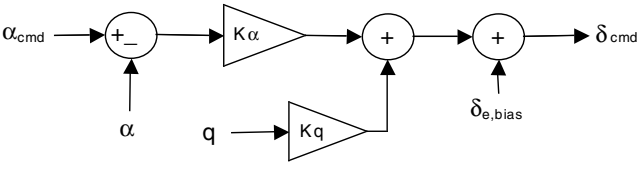

Fig. 21 Feedback control system implemented in ConSep.

Table 5 Summary of LGBB-bimese simulations

Description	LGBB-Mach 3 staging vehicle	LGBB-Mach 6 staging vehicle
Baseline	No active control, no separation motors	No active control, no separation motors
Nominal	Active PD control, no separation motors; $K_\alpha = -3$, $K_q = 8$, and $\alpha_{\text{cmd}} = 2.0$ deg	Active control of elevons, separation of 750,000 lb; $K_\alpha = -5$, $K_q = 5$, and $\alpha_{\text{cmd}} = 2.0$ deg
Parameter variations	Mass, inertia, flight path angle, and altitude at staging	Mass, inertia, flight path angle, and altitude at staging
Monte Carlo runs	Nominal separation parameters with aerodynamic uncertainties	None

III. Results and Discussion

A. Baseline Separation

The Mach 3 and Mach 6 separation trajectories with zero elevon deflections and zero separation thrust are presented in Figs. 19 and 20. These two cases are termed baseline separations. The simulation time was selected as 6 s, with an integration step size of 0.01 s. This duration and step size were considered satisfactory for the simulation of the stage separations discussed in this study.

For both Mach 3 and Mach 6 staging, each vehicle experiences positive normal force coefficient and positive pitching moment coefficients in the mated conditions (Figs. 11 and 14 for $\Delta x = \Delta z = 0$). As a result, when the forward joint was released at $t = 0.1$ s, the booster started to rotate nose-up about the aft joint and its angle of attack started slowly increasing. When the relative angle of attack reached 1.0 deg, the aft joint was released, setting the booster free. The two vehicles moved away from each other and separation distances Δx, Δz, and $\Delta\alpha$ kept increasing. However, the vehicle angles of attack went outside the database limits, violating the constraints.

B. Nominal Separation

To control the separations within the database limits, active closed-loop PD control of elevons was used for both Mach 3 and Mach 6 separations. Further, the separation thrusters were used for Mach 6 separation. No separation motors were used for Mach 3 separation. These two cases are termed nominal Mach 3 and Mach 6 separations.

A schematic diagram of the PD controller implemented in ConSep/ADAMS is shown in Fig. 21. The elevon deflections are now controlled by commanded angle of attack α_{cmd}, instantaneous angle of attack, elevon feedforward, and pitch rate feedback gains. In this study, the feedforward bias was not used. The full range of elevon deflection for which isolated LGBB test data were obtained is -30 to $+20$ deg. However, for nominal separation, the elevon

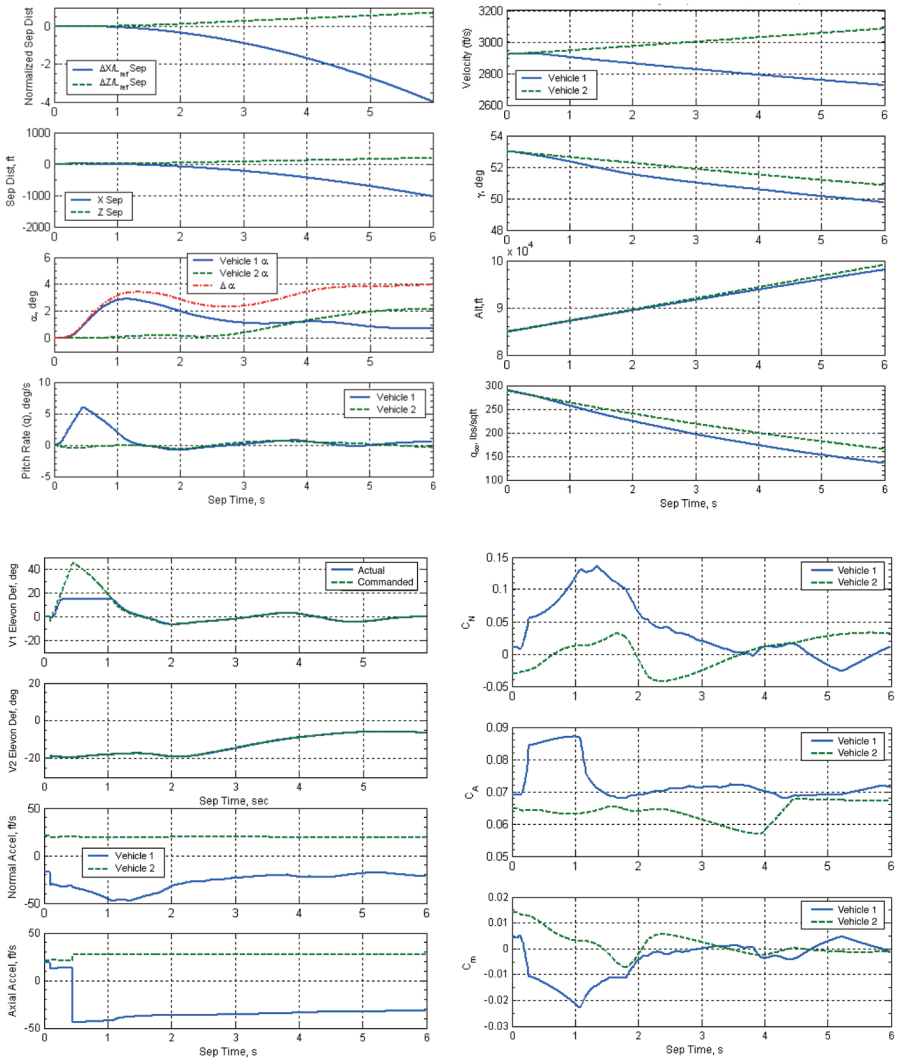

Fig. 22 Trajectory variables in Mach 3 nominal separation.

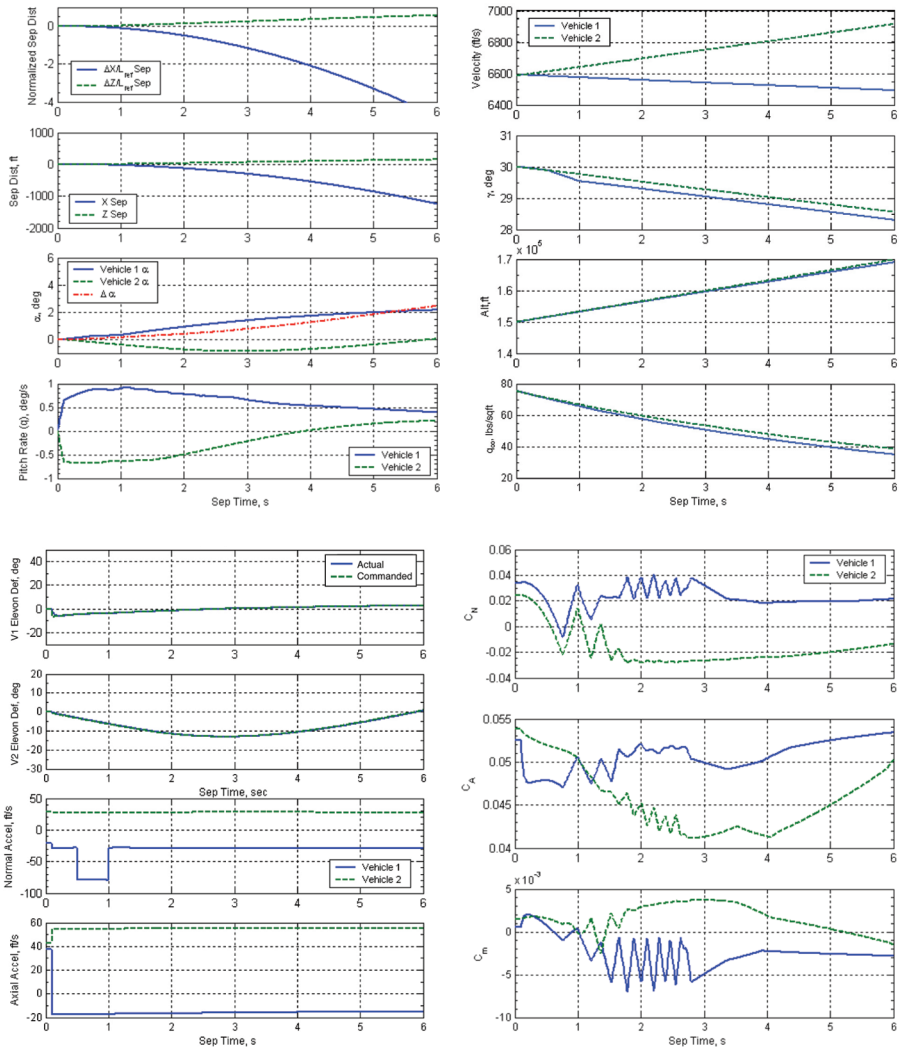

Fig. 23 Trajectory variables in Mach 6 nominal separation.

deflections were limited to −20 to +15-deg deflection to leave a margin for handling off-nominal conditions that are discussed later. The values of α_{cmd}, k_α, and k_q were determined by trial and error to keep the vehicles within the database limits. The nominal values of these parameters are presented in Table 5.

For Mach 3 staging, it can be observed from Fig. 22 that α and $\Delta\alpha$ remain within the limits of the proximity databases. The elevon deflections hit the specified limits initially but subsequently assume smaller values. The axial acceleration of the orbiter is positive due to a net positive thrust, but the booster experiences a negative acceleration (deceleration) due to drag. The booster has negative normal acceleration, but the orbiter has positive normal acceleration. These accelerations are measured in the body axes system of each vehicle. Because the z axis of the booster and the orbiter point toward each other [because they are in inverted positions (Fig. 5)], both vehicles tend to move in the same normal z direction. Because the orbiter is much heavier than the booster at staging, the magnitude of the orbiter's normal acceleration is much smaller than that of the booster. Therefore, the normal z separation distance between the two vehicles continues to increase with time. After 6 s, $\Delta x/l_{\text{ref}} = -4.0$ and $\Delta z/l_{\text{ref}} = 0.72$; that is, the booster is about 1038 ft aft of and 189 ft (6.6 diam) below the orbiter, and the two vehicles continue to move further apart. Therefore, for the LGBB-bimese vehicle, a successful Mach 3 staging is feasible using aerodynamic forces and moments acting on the booster and orbiter.

For Mach 3 staging, both booster and orbiter start with an initial velocity of 2924.6 ft/s and a flight path angle of 53.0 deg. At the end of 6 s, the velocities are, respectively, about 2725 ft/s and 3100 ft/s, corresponding to Mach numbers of about 2.8 and 3.2. The flight path angles are 50 and 51 deg, respectively, for the booster and the orbiter. As said before, the stage-separation wind-tunnel test data were based at Mach 3 and apply to cases in which the flight path angles of the booster and orbiter are equal. The issue of possible errors due to variations in Mach number and flight path angles is not addressed in this study.

For Mach 6 staging, simple aerodynamic staging was not feasible, apparently because the freestream dynamic pressure at 150,000-ft altitude is about one-fourth of that at 85,000-ft altitude for Mach 3 staging (see Table 4). Therefore, booster separation motors producing a combined thrust of 750,000 lb, acting for a duration of 0.5 s, immediately after the release of the aft joint were used. This thrust was assumed to be applied in the negative z_1 direction of the booster body-fixed coordinate system (Fig. 5). A higher magnitude of separation thrust certainly helps stage separation but increases the weight penalty due to the inclusion of separation motors. Using the performance and mass property data of the separation motors used on the solid rocket boosters of the space shuttle [19,20], the weight penalty of carrying the suite of separation motors producing a combined thrust of 750,000 lb for a duration of 0.5 s was estimated to be 5770 lb, which is about 1.92% of the booster weight at separation. The effect of separation motor plume impingement on proximity aerodynamic coefficients was not addressed in this study.

The combined use of active elevon control and separation motors results in a successful Mach 6 stage separation, as shown in Fig. 23. The nominal feedback control parameters for the Mach 6 separation are presented in Table 5. After 6 s, $\Delta x/l_{\text{ref}} = -4.8$ and

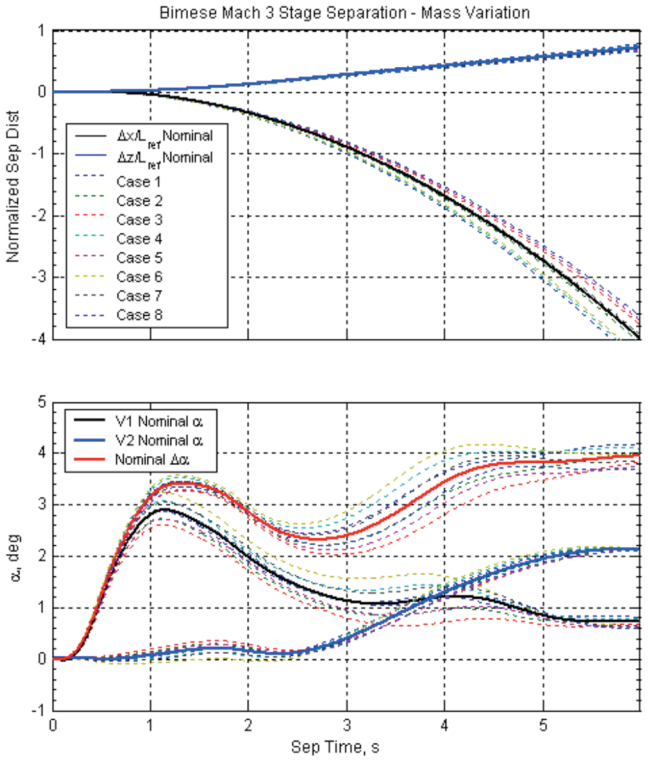

Fig. 24 Effect of parametric variation in vehicle mass.

$\Delta z/l_{\text{ref}} = 0.57$; that is, the booster is about 1250 ft aft of and 150 ft (5.2 diameters) below the orbiter and the two vehicles continue to move further apart.

For both Mach 3 and Mach 6 separations, large values of pitch rate feedback gains were required, particularly for the booster. This brought into question the role of C_{m_q} in the stage-separation simulations. The stage-separation test data for C_{mq} are not available. Using DATCOM methods [21] for the isolated LGBB vehicle at Mach 3, C_{mq} was estimated to be about -0.32 per radian; that is, about 200 times smaller than the artificial damping provided by the pitch rate feedback. Hence, no further efforts were made to include dynamic terms in the simulations performed in this study. A similar observation was made by Decker and Gera [5].

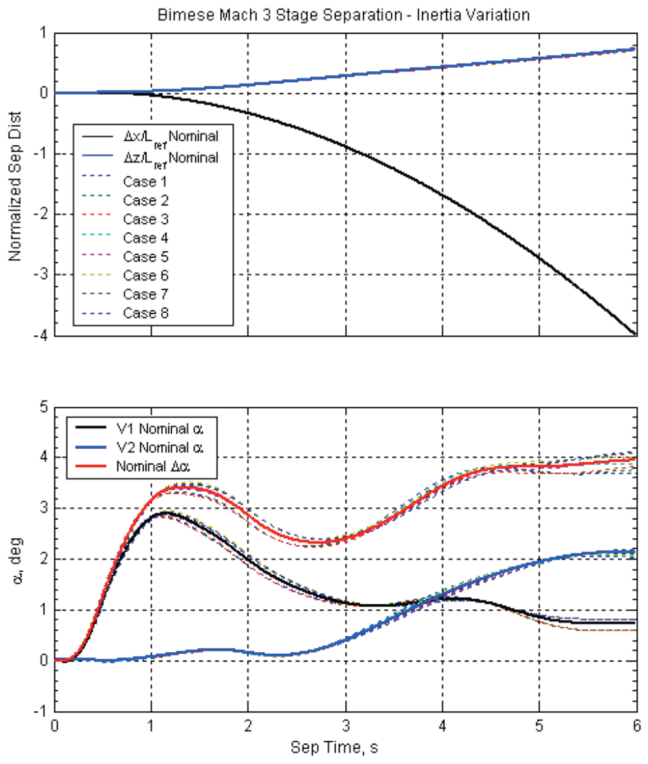

Fig. 25 Effect of parametric variation in pitch inertia.

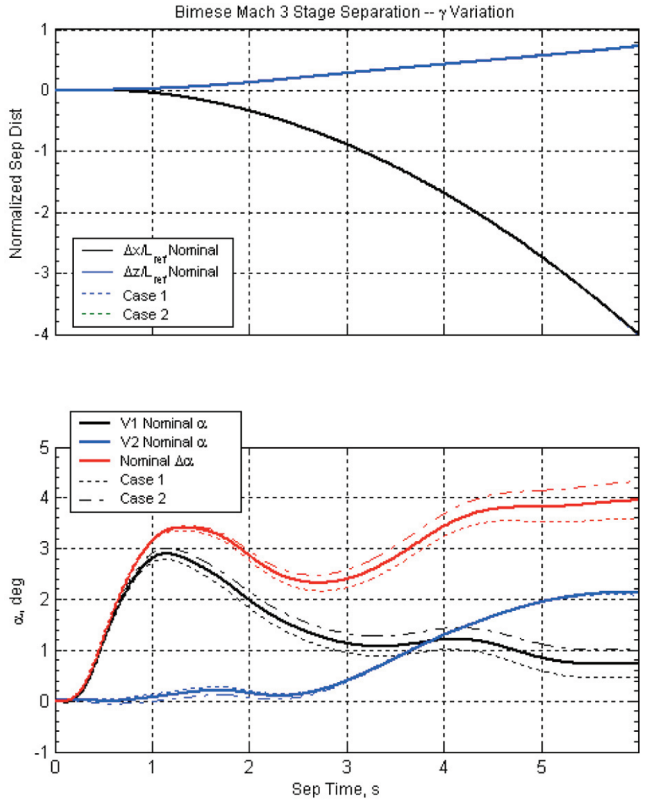

Fig. 26 Effect of parametric variations in flight path angle.

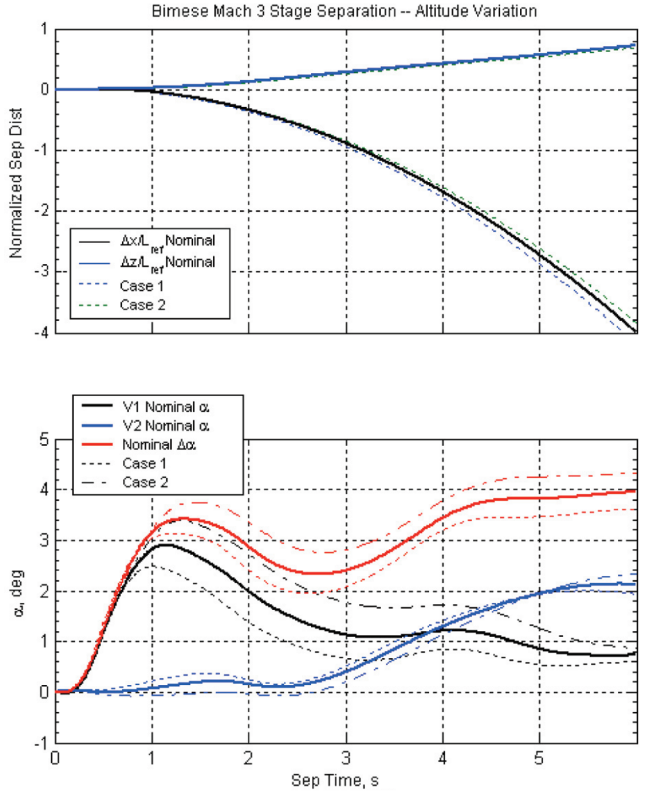

Fig. 27 Effect of parametric variation in altitude.

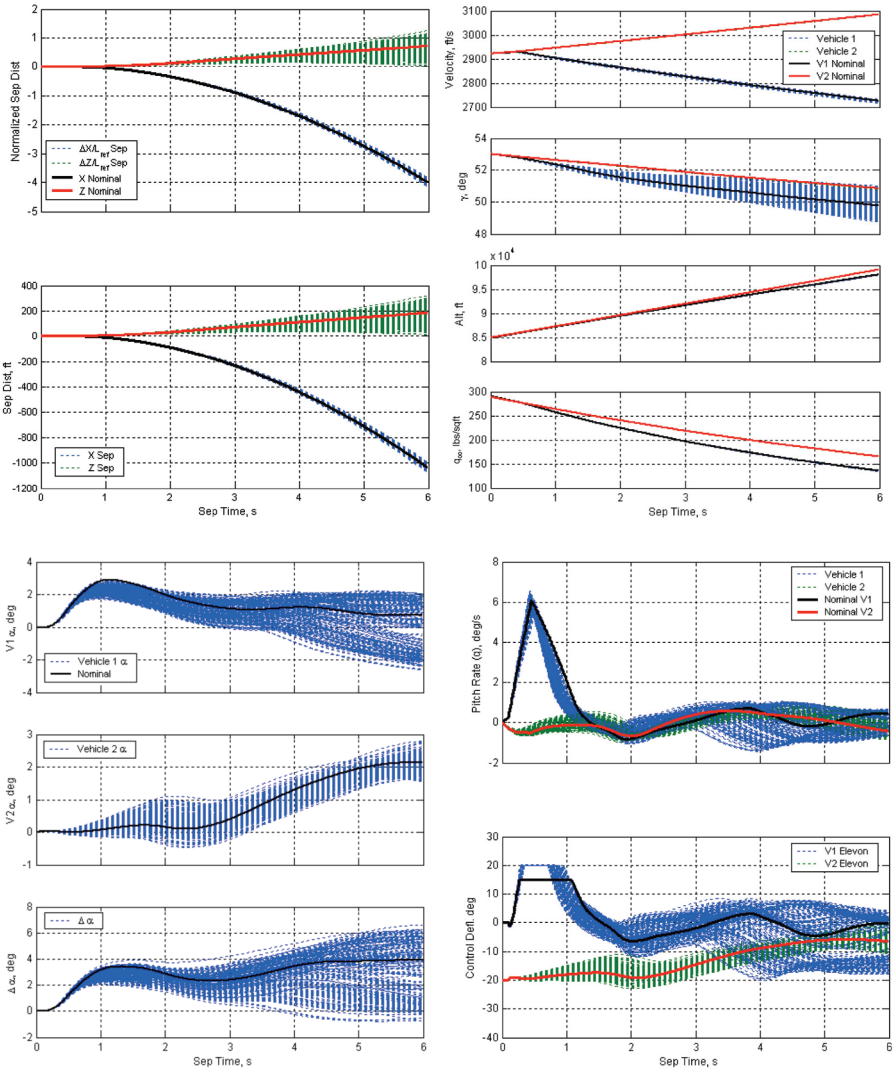

Fig. 28 Trajectory variables in 200 Monte Carlo runs for Mach 3 separation.

C. Effect of Parametric Variations

These studies were performed for both Mach 3 and Mach 6 staging LGBB-bimese vehicles. However, the results will be presented only for the Mach 3 staging LGBB-bimese vehicle, because the results were similar for the Mach 6 staging LGBB-bimese vehicle. The values of the feedback gains were held fixed at their nominal values, and the full range of elevon deflections were used for vehicle control during separation.

1. *Effect of Variation of Mass and Inertia*

The mass and inertia in pitch of both vehicles varied independently by $\pm 10\%$ from their nominal values, resulting in a combination of nine cases for each parameter. The results are shown in Figs. 24 and 25. It may be noted that the nominal Mach 3 feedback controller is capable of handling these variations in mass and inertia and keeping the vehicle α and $\Delta\alpha$ within the database limits.

2. *Effect of Variations in Flight Path Angle and Altitude at Staging*

The nominal values of flight path angle and altitude at staging are 53 deg and 85,000 ft, respectively. These were varied by ± 10 deg and ± 5000 ft, respectively. The results are shown in Figs. 26 and 27. It is noted that these variations can be handled by the nominal Mach 3 feedback controller satisfactorily and maintain the vehicle α and $\Delta\alpha$ within the database limits.

D. Monte Carlo Runs

These studies were performed to evaluate the robustness of the nominal controller to aerodynamic uncertainties when all the other parameters assumed their nominal values. Following a recent study on aerodynamic uncertainties of the X-33 vehicle [22] and the space shuttle heritage [23–25], two types of aerodynamic uncertainties were assumed: tolerances and variations. The tolerances are associated with measurement errors in wind tunnels. The estimated tolerances for Mach 3 stage-separation wind-tunnel testing are $C_N = \pm 0.0019$, $C_A = \pm 0.0012$, and $C_m = \pm 0.00022$. The data suitable for the estimation of variations in the stage-separation environment are not available. In the absence of a better alternative, the uncertainties associated with space shuttle reentry flight are used as variances in this study: $C_N = \pm 0.015$, $C_A = \pm 0.006$, and $C_m = \pm 0.003$. The total or net uncertainties were assumed to be the sum of tolerances and variances. It may be noted that these uncertainties are very conservative and are often as large as the proximity aerodynamic coefficients themselves.

The results of 200 Monte Carlo runs are presented in Fig. 28. The number of cases that resulted in successful separation ($\Delta z / l_{\text{ref}} \geq 0.2$) was 184 and the number of failures ($\Delta z / l_{\text{ref}} \leq 0.2$) was 16. The number of cases that went outside the database limits ($\Delta\alpha > 5.0$ deg) was 51, with a maximum $\Delta\alpha$ of 6.59 deg. However, for these 51 cases, the vehicle α were within the 5-deg limit. Considering that the estimated uncertainties were very much on the conservative side, it is believed that the nominal

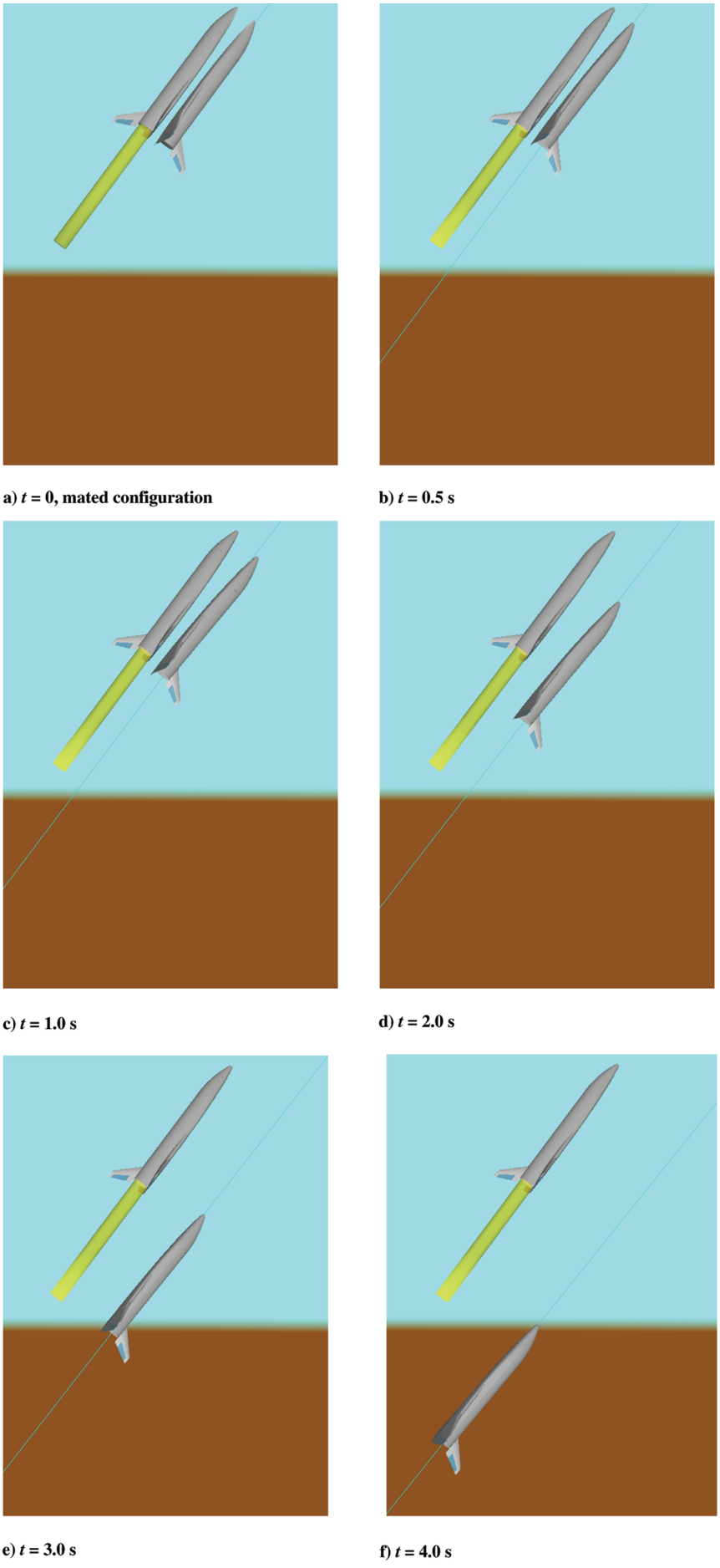

a) $t = 0$, mated configuration

b) $t = 0.5$ s

c) $t = 1.0$ s

d) $t = 2.0$ s

e) $t = 3.0$ s

f) $t = 4.0$ s

Fig. 29 Selected snapshots showing the relative locations of the booster orbiter during Mach 3 nominal separation.

controller for the Mach 3 staging satisfactorily handles the aerodynamic uncertainties assumed in this study.

E. Animation of the Staging Event

The ConSep output and the LGBB-bimese vehicle geometry models were input to SEE to produce animation of the staging event. As said before, the engine plume was assumed to be correctly expanded for both Mach 3 and Mach 6 operating altitudes and was modeled as a solid cylinder extending a few diameters from the base of the orbiter. Snapshots of the animation taken at selected time intervals are shown in Fig. 29.

IV. Conclusions

The analyses and simulation of the staging maneuvers of two TSTO vehicle concepts, one staging at Mach 3 and the other staging at Mach 6, were performed to demonstrate the application of the ConSep tool that is being developed as a part of NASA's stage-separation tool development activity. The proximity aerodynamic databases were developed using the data from stage-separation wind-tunnel tests conducted at NASA Langley Research Center. A passive release of the vehicles for Mach 3 and Mach 6 staging violated the constraint that the vehicle angles of attack and relative angles of attack remain inside the aerodynamic database limits. For a Mach 3 LGBB-bimese vehicle, aerodynamic separation subject to this constraint was feasible using active closed-loop feedback controller. However, for a Mach 6 LGBB-bimese vehicle, such an aerodynamic staging was not feasible and separation motors were used. Parametric variations in mass, inertia, flight path angle, and altitude at staging were investigated. Monte Carlo simulations were performed to evaluate the robustness of the nominal controller to aerodynamic uncertainties. The results indicate that the nominal controller satisfactorily handles off-nominal conditions in mass, inertia, flight path angle, altitude at staging, and estimated uncertainties in aerodynamic coefficients.

Acknowledgments

The authors gratefully acknowledge Wayne J. Borderlon and Alonzo L. Frost for NASA Marshall Space Flight Center stage-separation test data and schlieren photographs, Roger Lepsch for NASA Intercenter Systems Analysis Team vehicle concepts, Steve Harris and Mark McMillin for geometry, Paul Tartabini for ascent trajectory, and Scott Angster for animations.

References

[1] Dillenius, M. F. E., Perkins, S. C., and Nixon, D., "Pylon Carriage and Separation of Stores," *Tactical Missile Aerodynamics*, edited by M. J. Hemsch, Vol. 141, Progress in Astronautics and Aeronautics, AIAA, Washington, D.C., 1992.

[2] Taylor, R. T., and Alford, W. J, Jr., "A Wind Tunnel Investigation of the Carry Loads and Mutual Interference Effects of 1/40-Scale Models of the X-15 and B-52 Airplanes in Combination," NASA TM X-184, Dec. 1959.

[3] Decker, J. P., and Wilhite, A. W., "Technology and Methodology of Separating Two Similar Size Aerospace Vehicles Within the Atmosphere," AIAA Paper 1975-29, Jan. 1975.

[4] Decker, J. P., "Experimental Aerodynamics and Analysis of the Stage Separation of Reusable Launch Vehicles," NASA SP-148, Jan. 1967.

[5] Decker, J. P., and Gera, J., "An Exploratory Study of Parallel-Stage Separation of Reusable Launch Vehicles," NASA TN D-4765, Oct. 1968.

[6] Decker, J. P., "Aerodynamic Interference Effects Caused by Parallel-Staged Simple Aerodynamic Configuration at Mach Numbers of 3 and 6," NASA TN D-5379, Aug. 1969.

[7] Wilhite, A. W., "Analysis of Separation of the Space Shuttle Orbiter from a Large Transport Airplane," NASA TM X-3492, June 1977.

[8] Naftel, J. C., and Wilhite, A. W., "Analysis of Separation of a Two-Stage Winged Launch Vehicle," AIAA Paper 86-0195, Jan. 1986.

[9] Naftel, J. C., and Powell, R. W., "Aerodynamic Separation and Glideback of a Mach 3 Staged Orbiter," AIAA Paper 90-0223, Jan. 1990.

[10] Naftel, J. C., and Powell, R. W., "Analysis of the Staging Maneuver and Booster Glideback Guidance for a Two-Staged, Winged, Fully Reusable Launch Vehicle," NASA TP-3335, 1993.

[11] Pamadi, B. N., Tartabini, P. V., and Starr, B. R., "Ascent, Stage Separation and Glideback Performance of a Partially Reusable Small Launch Vehicle," AIAA Paper 2004-0876, 2004.

[12] Murphy, K. J., Buning, P. G., Pamadi, B. N., Scallion, W. I., and Jones, K. M., "Status of Stage Separation Tool Development for Next Generation Launch Vehicle Technologies," AIAA Paper 2004-2595, 2004.

[13] Pamadi, B. N., Neirynck, T. A., Covell, P. F., Hotchko, N. J., and Bose, D. M., "Simulation and Analyses of Staging Maneuvers of Next Generation Reusable Launch Vehicles," AIAA Paper 2004-5185, 2004.

[14] Bordelon, W. J., Frost, A. L., and Reed, D. K., "Stage Separation Wind Tunnel Tests of a Generic Two-Stage-to-Orbit Launch Vehicle," AIAA Paper 2003-4227, July 2003.

[15] Anon., *Using ADAMS/Solver*, Mechanical Dynamics, Inc.,, Mesa, AZ, 1999.

[16] Tartabini, P. V., Bose, D. M., McMinn, J. D., Martin, J. G., and Stovers, B. K., "Hyper-X Stage Separation Trajectory Validation Studies," AIAA Paper 2003-5819, 2003.

[17] Bose, D. M., and Hotchko, N., "Conceptual Level Stage Separation Simulation (ConSep): Version 1.1 User's Guide," Analytical Mechanics Associates, Rept. 02-37 Rev. B, Hampton, VA, Dec. 2003.

[18] Angster, S., "Synergistic Engineering Environment Build 2 User's Guide, Revision E," Analytical Mechanics Associates, Rept. 03-31, Hampton, VA, Aug. 2003.

[19] Anon., " Performance Enhancement Operational Aerodynamic Design Data Book," Boeing, Rept. RSS98D0313, Jan. 1999.

[20] Anon., STS36: SRB Preflight Predicted Mass Properties. SRB Mass Properties , NASA Marshall Space Flight Center, Rept. 64, Addendum D, Dec. 1989.

[21] Pamadi, B. N., *Performance, Stability, Dynamics and Control of Airplanes*, 2nd ed., AIAA Education Series, AIAA, Reston, VA, 2004, pp. 174–175, 187–188.

[22] Cobleigh, Brent R., "Development of the X-33 Aerodynamic Uncertainty Model," NASA TP-1998-206544, Apr. 1998.

[23] Young, James C., and Underwood, Jimmy M., "The Development of Aerodynamic Uncertainties for the Space Shuttle Orbiter," AIAA Paper 82-0563, 1982.

[24] Anon., "Reusable Space Systems/United Space Alliance, Orbiter Operational Aerodynamic Data Book," Boeing, Rept RSS99D0001, Apr. 2000.

[25] Anon., "Aerodynamic Design Data Book," Vol. 1, Rockwell International Space Div., Rept. 772-SH-0060-1L, Downey, CA, Nov. 1977.

P. Huseman
Associate Editor